SUPPLEMENTAL MATERIAL

Scally et al., https://doi.org/10.1084/jem.20170869

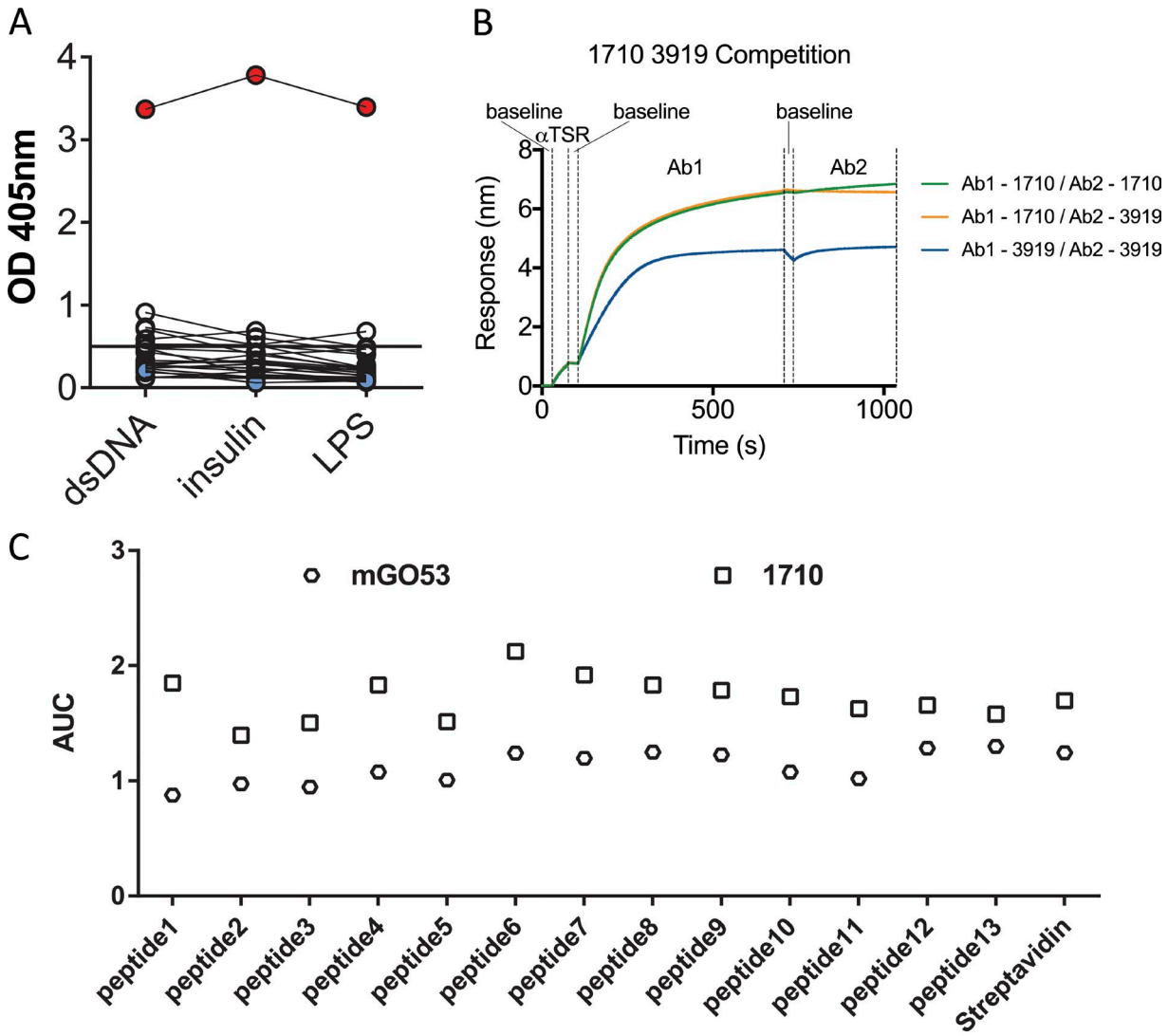

Peptide	Sequence	Peptide	Sequence
peptide1	NKNNQGNGQGHNMP	peptide7	NKIQNSLSTEWSPC
peptide2	QGHNMPNDPNRNVD	peptide8	TEWSPCSVTCGNGI
peptide3	PNRNVDENANANSA	peptide9	TCGNGIQVRIKPGS
peptide4	ANANSAVKNNNNEE	peptide10	RIKPGSANKPKDEL
peptide5	NNNNEEPSDKHIKE	peptide11	KPKDELDYANDIEK
peptide6	DKHIKEYLNKIQNS	peptide12	ANDIEKKICKMEKC
		peptide13	MEKCSSVFNVVNSS

Figure S1. **Characterization of C-PfCSP binding to C-PfCSP–reactive antibodies. (A)** Polyreactivity assessment of C-PfCSP–binding antibodies. C-PfCSP–reactive antibodies were tested for polyreactivity by binding to three different antigens: dsDNA, insulin, and LPS (Wardemann et al., 2003). ED38 (red) and mGO53 (blue) were used as positive and negative controls, respectively. Horizontal line indicates the cutoff OD_{405} for positive reactivity for the corresponding antigen. Data are representative of two independent experiments. **(B)** Competition binding data for 1710 and 3919. Sensorgram for competition binding studies of 1710 and 3919 IgG to the αTSR (NF54) PfCSP construct. The His-tagged αTSR domain was first bound to NiNTA biosensors followed by a baseline equilibration. 1710 (green and yellow) or 3919 (blue) were next allowed to bind the antigen. After a baseline step, biosensors were dipped in a competing antibody well (1710, green; 3919, yellow and blue). 1710 competed with 3919 for binding to the αTSR domain, indicating they share a similar or overlapping binding site. **(C)** 1710 and isotype control mGO53 were screened for binding to the indicated linear C-PfCSP peptides. Area under the curve is calculated for ELISA curves as in Fig. 1 (B and C). Data are representative of two independent experiments.

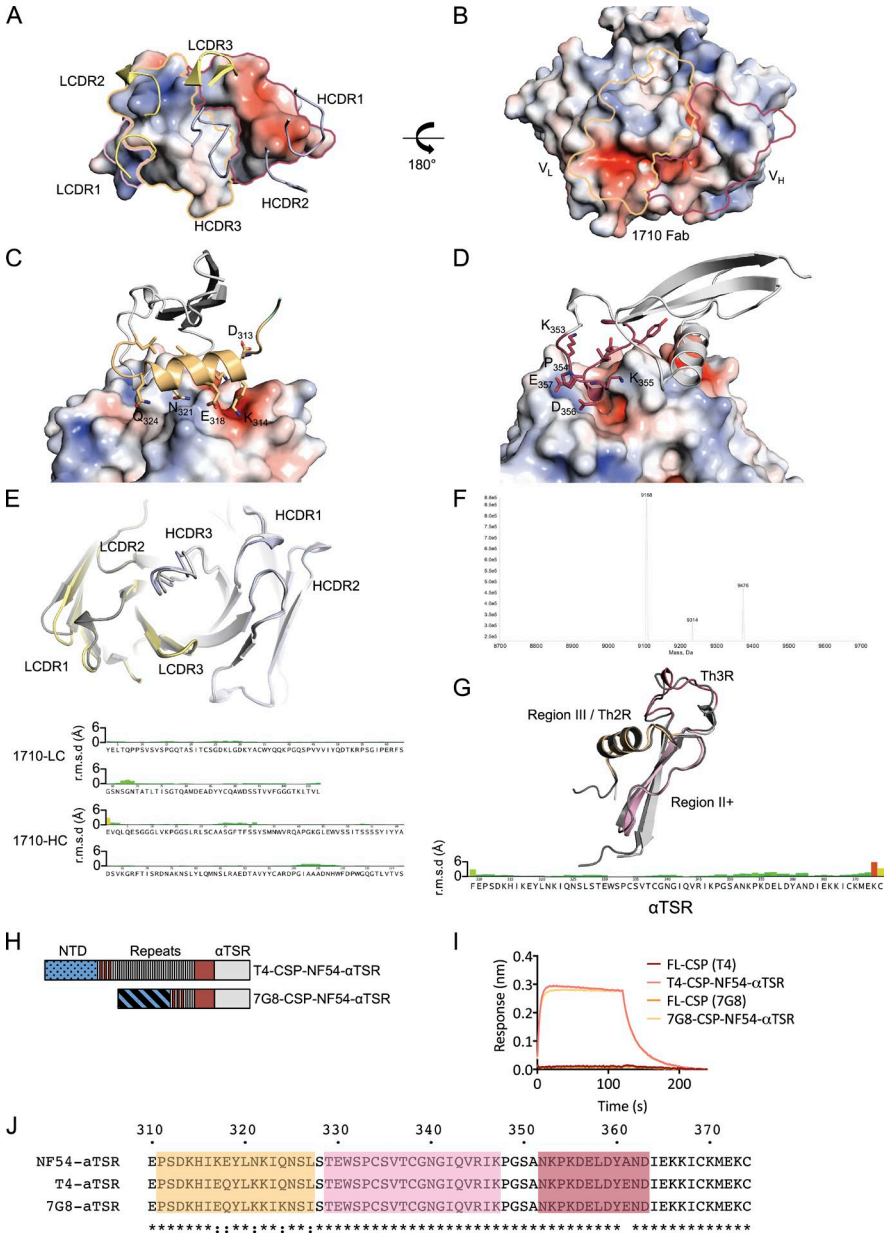

Figure S2. **Structural and biophysical analysis of 1710 and PfCSP αTSR. (A–D)** Electrostatics of the 1710 paratope and αTSR epitope. The solvent accessible electrostatic potential for αTSR (A) and 1710 Fab (B). The Th2R, Th3R, and region II+ regions are outlined in orange, maroon, and pink, respectively. Region II+ is not outlined in B as it does not interact with 1710. The solvent accessible electrostatic potential of 1710, showing interacting residues from the Th2R (C) and Th3R (D) epitopes of αTSR, is shown as a cartoon representation. Electrostatic calculations were performed using APBS (Baker et al., 2001; ±5 *kT/e*). **(E)** Superposition of unliganded and αTSR-bound 1710 Fab structures. 1710 Fab LCDRs and HCDRs bound to αTSR are yellow and blue, respectively, with the unliganded 1710 Fab CDRs in gray. The r.m.s.d. (Cα's) between the variable chains of the C-CSP–bound 1710 Fab and unliganded 1710 Fab are plotted, and indicate that there is little main chain movement between the two structures. The 1710 paratope is largely pre-configured in its binding-competent conformation. The r.m.s.d. between the two superposed structures was calculated using MOE 2015.10 (MOE, 2013). **(F)** ESI/TOF mass spectra of the HEK293F-expressed NF54 αTSR. Three major peaks were observed, corresponding to non-glycosylated αTSR (9,168 Da), and two O-fucosylated products, one with an O-fucose (9,314 Da, +146 Da) and a heavier species with an O-glucosylfucose disaccharide (9,476 Da, +308 Da). **(G)** Superposition of the 1710-bound αTSR and unliganded αTSR (PDB ID: 3VDJ). αTSR bound to 1710 is light gray, with the Th2R, region II+, and Th3R in orange, pink and maroon, respectively, whereas the unliganded αTSR is dark gray. The r.m.s.d. (Cα's) between the two superposed structures is shown as bar graphs for each αTSR residue and was calculated using MOE 2015.10 (MOE, 2013). **(H)** Schematic representation of the chimeric FL PfCSP constructs used in binding studies. **(I)** 1710 Fab binding to T4 and 7G8 chimeric FL PfCSP constructs in which the αTSR domain was substituted with the NF54 sequence. Data are representative of two independent measurements. **(J)** Sequence alignment of the NF54, T4 and 7G8 αTSR PfCSP sequences generated using Clustal Omega (Sievers et al., 2011). Region III/Th2R, region II+, and Th3R are in orange, pink and maroon, respectively. NTD, N-terminal domain.

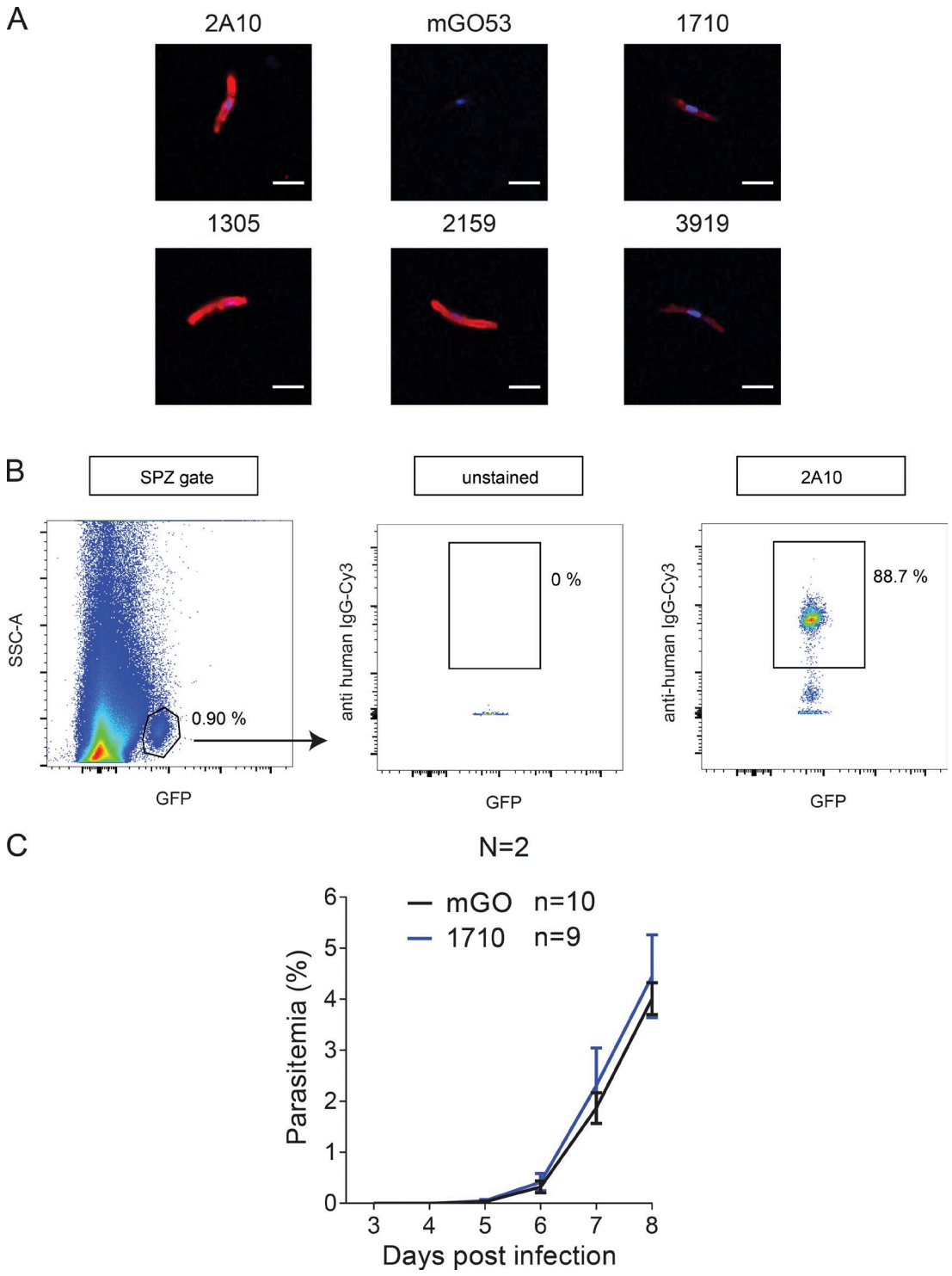

Figure S3. ***Pb-PfCSP* sporozoite binding and functional evaluation of C-PfCSP antibodies. (A)** Representative immunofluorescence images of fixed Pf NF54 salivary gland sporozoites stained with the indicated C-PfCSP–reactive antibodies (red) and DAPI (nuclei, blue). 1305 and 2159 are isolated C-PfCSP–binding antibodies that also cross-react with the NANP repeat (see Fig. 1). 2A10 and mGO53 were used as positive and negative control, respectively. Bars, 5 µm. **(B)** Flow cytometric gating strategy of GFP-positive *Pb-PfCSP* sporozoites with indicated frequencies exemplified by 2A10 (Triller et al., 2017). (A and B) Data are representative of two independent experiments. **(C)** Mean blood parasitemia from days 3–7 after infection with *Pb-PfCSP* transgenic sporozoites in mice passively immunized with 1710 or mGO53. N indicates the number of mice that developed parasitemia in each group. Data are from two independent experiments. Error bars indicate standard error of the mean.

Table S1. **Data collection and refinement statistics for 1710 Fab–αTSR and unliganded 1710 Fab crystal structures**

Parameter	1710 Fab–αTSR	1710 Fab
Wavelength (Å)	0.97948	0.97949
Space group	$P2_12_12_1$	$P2_12_12_1$
Cell dimensions		
a,*b*,*c* (Å)	70.49, 70.68, 96.28	61.06, 66.72, 124.03
α, β, γ (°)	90, 90, 90	90, 90, 90
Resolution (Å)[a]	39.79–1.95 (2.05–1.95)	45–1.9 (2.00–1.90)
No. molecules in ASU	1	1
No. unique observations	35,815 (4,909)	40,776 (5,691)
Multiplicity	7.4 (7.4)	5.4 (5.3)
R_{merge} (%)[b]	15.7 (70.3)	9.4 (61.9)
R_{pim} (%)[c]	6.2 (29.5)	4.4 (28.9)
<I/σ I>	11.6 (1.7)	13.2 (1.9)
Completeness (%)	100 (100)	99.5 (99.2)
$CC_{1/2}$	99.6 (56.8)	99.8 (64.7)
Refinement statistics		
Nonhydrogen atoms	4,145	3,544
Macromolecule	3,715	3,244
Water	377	240
Ligand	34	60
R_{factor}[d]/R_{free}[e]	18.0/22.3	18.4/22.0
Rms deviations from ideality		
Bond lengths (Å)	0.003	0.005
Bond angle (°)	0.65	0.77
Dihedrals (°)	13.0	13.6
Ramachandran plot		
Favored regions (%)	97.3	97.2
Allowed regions (%)	2.7	2.8
B-factors (Å^2)		
Average B-factors	26.1	35.5
Average macromolecule	25.3	34.6
Average ligands	47.9	52.8
Average water	32.2	43.2

[a]Values in parentheses refer to the highest resolution bin.
[b]$R_{merge} = \sum hkl \sum i \mid Ihkl, i - \langle Ihkl \rangle \mid / \Sigma hkl \langle Ihkl \rangle$.
[c]$R_{pim} = \sum hkl [1/(N-1)]1/2 \sum i \mid Ihkl, i - \langle Ihkl \rangle \mid / \sum hkl \langle Ihkl \rangle$.
[d]$R_{factor} = (\sum \mid |Fo| - |Fc| \mid) / (\sum \mid |Fo|)$ for all data except as indicated in footnote e.
[e]5% of data were used for the R_{free} calculation.

REFERENCES

Baker, N.A., D. Sept, S. Joseph, M.J. Holst, and J.A. McCammon. 2001. Electrostatics of nanosystems: application to microtubules and the ribosome. *Proc. Natl. Acad. Sci. USA.* 98:10037–10041. https://doi.org/10.1073/pnas.181342398

MOE. 2013. Molecular Operating Environment (MOE), 2013.08. *Chemical Computing Group*. Available at: https://www.chemcomp.com/MOE2013.htm

Sievers, F., A. Wilm, D. Dineen, T.J. Gibson, K. Karplus, W. Li, R. Lopez, H. McWilliam, M. Remmert, J. Söding, et al. 2011. Fast, scalable generation of high-quality protein multiple sequence alignments using Clustal Omega. *Mol. Syst. Biol.* 7:539. https://doi.org/10.1038/msb.2011.75

Triller, G., S.W. Scally, G. Costa, M. Pissarev, C. Kreschel, A. Bosch, E. Marois, B.K. Sack, A.M. Salman, C.J. Janse, et al. 2017. Protective human anti-malarial antibodies induced by natural exposure. *Immunity*. https://doi.org/10.1016/j.immuni.2017.11.007

Wardemann, H., S. Yurasov, A. Schaefer, J.W. Young, E. Meffre, and M.C. Nussenzweig. 2003. Predominant autoantibody production by early human B cell precursors. *Science*. 301:1374–1377. https://doi.org/10.1126/science.108690712920303